Schweizerische Eidgenossenschaft
Confédération suisse
Confederazione Svizzera
Confederaziun svizra

Federal Department of the Environment, Transport, Energy and Communications DETEC

Swiss Federal Office of Energy SFOE
Energy Research and Cleantech Division

REEL Demo – Romande Energie ELectric network in local balance Demonstrator

Deliverable: 4f3 Validation of the Model On the Demonstration (RE Demo): Optimal Scheduling and Control of Active Distribution Networks for Power Flexibility Provision at TSO-DSO Interface

Demo site: Aigle

Developed by
Mohsen Kalantar Neyestanaki, EPFL-PWRS
Rachid Cherkaoui, EPFL-PWRS
in collaboration with
Swissgrid

[Lausanne, 27.09.2020]

Contents

1. Description of deliverable and goal

1.1. Executive summary

Relying on the power flexibility of distributed energy resources (DERs) located in an active distribution network (ADN), this ADN could be able to provide power flexibility to the transmission system at their point of common coupling (PCC). The power flexibility is defined as additional bi-directional active/reactive powers a resource can provide to the grid by adjusting its operating point. In this respect, this report presents a two-stage method to firstly schedule and then control an ADN to provide power flexibility at the PCC. Based on the power flexibility request of the transmission system operator (TSO), the first stage determines the optimal amount of power flexibility that an ADN operator should procure from each DER considering the corresponding offer curves as well as the uncertainties stemming from the short-term forecast errors of demand and renewable generation. The constraints and losses of the grid are accounted for by exploiting a linearized power flow model, whereby the first stage is implemented as a linear scenario-based optimization problem. Then, in real-time operation, relying on a linear optimization problem, the second stage adjusts the power flexibility injection of a battery energy storage system (ESS) to mitigate the imbalance at the PCC inherent in the above-mentioned uncertainties. The performance of the proposed method is tested in the case of a real ADN located in the city of Aigle in southwest of Switzerland.

1.2. Research question

Environmental challenges along with the recent developments in renewable energy technologies have launched a fast trend toward a CO2- and nuclear waste-free electricity generation future [1], [2]. For example, in Switzerland with around 38% nuclear electricity generation, it has been planned to shut down all nuclear plants by 2050, thus opening the way for electricity generation from renewable energy sources [3]. Nevertheless, in order to realize this goal, a rapt attention should be devoted to the power flexibility provision issue to guarantee that enough regulation capacity is available for voltage/frequency regulation to compensate the variability of stochastic renewable energy resources like solar and wind [4], [5].

Tracking the evolution of distribution networks from passive to active ones illustrates that the number of distributed energy resources (DERs) they are accommodating is rapidly increasing [6]. In order to keep the security and quality of supply in this emerging architecture, a solution is to deploy the power flexibility of DERs located in active distribution networks (ADNs) to provide it to the transmission systems [7]-[10]. This solution necessitates a tighter collaboration between transmission system operators (TSOs) and distribution system operators (DSOs) to exchange such a flexibility [11]. The active and reactive powers flexibility can be defined as additional bi-directional active/reactive powers a given resource (DER, ADN) can provide to the grid by regulating its operating point, i.e. increasing or decreasing its active/reactive powers consumption/generation. The **questions** that naturally arise in this context are:

1- how much are the ranges of active/reactive powers flexibility that an ADN can provide to the transmission system at their point of common coupling (PCC)?

2- how much should be the active/reactive powers flexibility provided by each DER in such a way that the ADN can provide the requested active/reactive powers flexibility of the TSO at the PCC?

1.3. Novelty of the proposed solutions compared to the state-of-art

In regard to the **first question**, the flexibility provision capability (FPC) curve of an ADN can be defined in a P-Q plane. An FPC curve refers to a planned operating point of the ADN and characterizes the extreme amount of active and reactive powers flexibility that the ADN can provide to the transmission system at the PCC. The area surrounded by the FPC curve is called FPC area. The work in [7] introduces a random sampling method to estimate the FPC area of an ADN. This method actually determines a set of points instead of the perimeter of the ADN's FPC area (FPC curve). This method is fundamentally an exhaustive search and inevitably has a high computational burden. The works in [8] and [9] are grounded on the solution of a non-convex non-linear optimal power flow problem to estimate the FPC curve of an ADN. They also lack the tractability properties due to their non-convex formulation. All the above-mentioned works neglect uncertainties, i.e. the forecast errors of demand and renewable generation, hence, their estimated FPC area might differ from the real one. To estimate the FPC area precisely, our work in [10] considers uncertainties and introduces a set of linear scenario-based robust optimization problem to estimate the FPC area.

Based on the methods proposed in [7]-[10], an ADN operator can offer to the TSO its FPC area (i.e. capability for flexibility provision) for each time slot of a specified time horizon (next day or next week). Then, based on and in case of need, the TSO sends to the ADN operator its active/reactive powers flexibility request for each upcoming time slot few minutes, let's call it t_{TSO} minutes, prior the beginning of that time slot. Then, the ADN operator optimally distribute that flexibility request of the TSO among all DERs located in its grid while considering the grid constraints, the power losses and the uncertainties. In other words, the ADN operator addresses **the second above-mentioned question**. To the best knowledge of the authors, the treatment of this question is missing in the literature known so far. Thus, this report aims at addressing that question to tackle the second challenge in the way of unlocking the flexibility of DERs located in the ADNs.

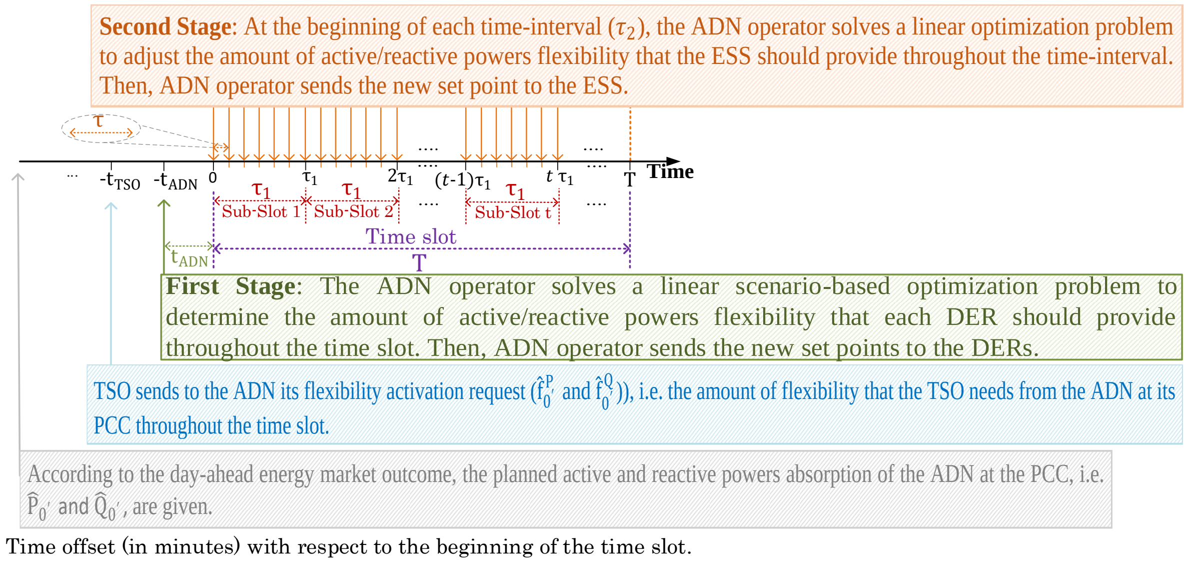

Fig. 1 The timeline of the proposed method for a time slot

1.4. Description

The method presented in this report consists of two stages: 1- the First stage is entitled scheduling stage. Few minutes, let's call it t_{ADN} minutes, prior the beginning of a time slot, it schedules the operating points of the DERs to satisfy as much as possible the flexibility request of the TSO at the PCC while minimizing the total cost of the ADN operator for flexibility procurement from the DERs and ensuring at best an adequate level of energy in the battery energy storage system (ESS) that will be used in the second stage. The first stage consists in an optimization problem that accounts for the power losses and grid constraints of the ADN using the linearized power flow model introduced in [12]. It explicitly models uncertainties with a set of scenarios, finally resulting in a linear scenario-based optimization problem. 2- The Second stage is entitled real-time control. In real-time operation, where the actual consumption /generation of the ADN's loads/renewable resources are realized and the DERs flexibility is deployed, this stage adjusts the active/reactive powers flexibility injection of the ESS to mitigate the deviations from the requested active/reactive powers flexibility of the TSO at the PCC. This stage is implemented based on a linear optimization problem considering the operational constraints of the ESS. In this way, it tries to mitigate the impact of uncertainties on the imbalance at the PCC over the whole time slot.

1.4.1. The architecture of the TSO-DSO collaboration

The architecture of the TSO-DSO collaboration for unlocking the flexibility of DERs located in ADNs might vary from system to system. This report opts for a general one, as demonstrated in Fig. 1, in order to be compatible with any desired architecture. The method presented in this report is grounded on the following considerations:

- the duration of each time slot is T minutes. It is formed of a number of sub-slots, each with duration of τ_1 seconds;

- on the basis of the day-ahead energy market outcome, the *planned operating point* of the ADN (see details in Section 1.4.2) is known with a time resolution of T, i.e. a unique operating point for each time slot;
- t_{TSO} minutes before the beginning of each time slot, TSO sends to the ADN operator its active/reactive powers flexibility request with reference to the planned operating point, for that time slot, thanks to the corresponding FPC area;
- the first stage of the proposed method determines the optimal amount of active/reactive powers flexibility that the ADN operator should procure from each DER throughout that time slot. It is a constant amount of flexibility from each DER over the whole time slot. However, it accommodates at best the temporal variations and uncertainties of the demand/renewable generation with time resolution of τ_1;
- t_{ADN} minutes before the beginning of each time slot, based on the outcome of the first stage of the method, the ADN operator sends to each DER its new set-point. In this way, it is compliant with the current regulations which entail sending to the providers, i.e. DERs, the flexibility request for each time slot in advance;
- the second stage starts at the beginning of the time slot and lasts until the end of the time slot. It splits each sub-slot into a number of time-intervals with duration of τ_2 seconds, i.e the time resolution of the real-time control strategy. At the beginning of each time-interval, it determines the active/reactive powers flexibility that the ESS should provide during that time-interval, whereby, the ADN operator adjusts the set-point of the ESS. In parallel and during the whole time slot, the DERs are operated according to their new constant set-points as mentioned previously.

1.4.2. FIRST STAGE: SCHEDULING METHODOLOGY

The targeted active/reactive power flow at the PCC of the ADN, i.e. $P_{0'}^{\mathrm{Target}}$ and $Q_{0'}^{\mathrm{Target}}$, consist of two terms:

$$P_{0'}^{\mathrm{Target}} = \widehat{P}_{0'} + \hat{f}_{0'}^{P}, \tag{1}$$

$$Q_{0'}^{\mathrm{Target}} = \widehat{Q}_{0'} + \hat{f}_{0'}^{Q}, \tag{2}$$

where $0'$ is the index for the PCC node; $\widehat{P}_{0'}$ and $\widehat{Q}_{0'}$ indicate the day-ahead *planned* active/reactive power absorption of the ADN at the PCC with time resolution of T (a unique value for the whole time slot); $\hat{f}_{0'}^{P}$ and $\hat{f}_{0'}^{Q}$ indicate the active/reactive powers flexibility requested by the TSO from the ADN at the PCC with time resolution of T (unique values for the whole time slot). The first stage of the method aims at determining the optimal amount of active/reactive powers flexibility that the ADN operator should procure from each DER in order to follow the targeted power flow at the PCC with minimum cost and deviation. In this way, it changes the

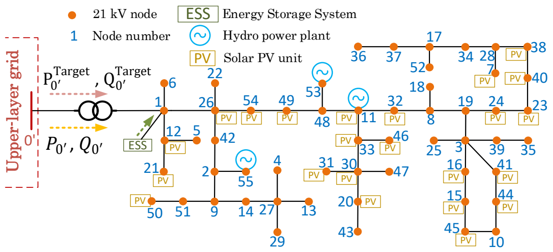

Fig. 2 The single line diagram of an active distribution network located in Aigle (a city in southwest of Switzerland).

nodal active/reactive power injections to economically satisfy the targeted power flow at the PCC of the ADN.

To formulate the scheduling problem, let us first introduce i and j as the indices for the nodes excluding the PCC node, i.e. $0'$; $\mathbb{B}$ as the set of nodes excluding $0'$; t and t' as the indices for the sub-slots; $\mathbb{T}$ as the set of sub-slots belonging to time slot T; s as the index for scenarios modeling the forecast errors of demand and renewable generation; $\mathbb{S}$ as the set of selected credible scenarios; l as the index for the branches; $\mathbb{L}$ as the set of branches of the ADN; k as the index for the dispatchable distributed generators (DDGs); $\mathbb{DDG}_i$ as the set of DDGs connected to node i; $\mathbb{DDG}$ as the set of DDGs located in the ADN; h as the index for the renewable distributed generators (RDGs); $\mathbb{RDG}_i$ as the set of RDGs connected to node i; $\mathbb{RDG}$ as the set of RDGs located in the ADN.

Although the formulation presented here is generic, it is assumed that:

- each DDG has only a single set-point over the whole time slot T;
- DDGs can provide active and reactive powers flexibility, i.e. $f_k^{\mathrm{DDG,P}}$ and $f_k^{\mathrm{DDG,Q}}$, in addition to their *planned* active/reactive power injections, i.e. $\widehat{\mathrm{P}}_k^{\mathrm{DDG}}$ and $\widehat{\mathrm{Q}}_k^{\mathrm{DDG}}$;
- the trajectory of the *forecasted* active power injection of the RDGs, i.e. $\widehat{\mathrm{P}}_{ht}^{\mathrm{RDG}}$, are considered with time resolution of τ_1;
- the *planned* reactive power injection of RDGs, i.e. $\widehat{\mathrm{Q}}_h^{\mathrm{RDG}}$, are assumed to be 0;
- RDGs are sources of active power uncertainties, i.e. $\Delta\mathrm{P}_{hts}^{\mathrm{RDG}}$. Thus, they might deviate from their *forecasted* active power injection $\widehat{\mathrm{P}}_{ht}^{\mathrm{RDG}}$. However, they can provide reactive power flexibility, i.e. $f_h^{\mathrm{RDG,Q}}$, in addition to their *planned* reactive power injection $\widehat{\mathrm{Q}}_h^{\mathrm{RDG}}$;
- the trajectory of the *forecasted* active/reactive power absorptions of loads, i.e. $\widehat{\mathrm{P}}_{it}^{\mathrm{D}}$ and $\widehat{\mathrm{Q}}_{it}^{\mathrm{D}}$, are considered with time resolution of τ_1;
- loads are sources of active/reactive power uncertainties, i.e. $\Delta\mathrm{P}_{its}^{\mathrm{D}}$ and $\Delta\mathrm{Q}_{its}^{\mathrm{D}}$.Thus, they might deviate from their *forecasted* active/reactive power absorptions, i.e. $\widehat{\mathrm{P}}_{it}^{\mathrm{D}}/\widehat{\mathrm{Q}}_{it}^{\mathrm{D}}$;
- the forecast errors of renewable generation and demand, i.e. $\Delta\mathrm{P}_{hts}^{\mathrm{RDG}}$, $\Delta\mathrm{P}_{its}^{\mathrm{D}}$ and $\Delta\mathrm{Q}_{its}^{\mathrm{D}}$ are modeled through a set of scenarios with time resolution of τ_1;
- the ADN hosts an ESS at its root, i.e. node 1 shown in Fig. 2, as a sole real-time controllable resource. The ESS is fully dedicated to the real-time control stage and its *planned*

active/reactive power injections are 0;

- the first stage keeps the reactive power flexibility provision of the ESS equal to zero to make free all the capacity of the ESS for the active power flexibility provision. It determines the required active power flexibility from the ESS, i.e. $f_{ts}^{\mathrm{ESS,P}}$, during each sub-slot t and scenario s. $f_{ts}^{\mathrm{ESS,P}}$ consists in the sum of two terms, $P^{\mathrm{ESS,Restore}}$ and $F_{ts}^{\mathrm{ESS,P}}$. To empower the ESS to provide flexibility during the second stage, the first stage schedules the set-point of the ESS, i.e. $P^{\mathrm{ESS,Restore}}$, over the whole time slot such that the ESS restores an adequate level of energy. For each individual scenario s, F_{ts}^{ESS} indicates the final adjustment of the ESS's set-point over sub-slot t that is expected to be accomplished by the ADN operator during the second stage.

The scheduling methodology is modeled based on a linear scenario-based optimization problem as detailed in the following.

A) Calculating the State of the Grid

Procuring the flexibility of DERs changes the nodal active/reactive power injections, whereby the state of the grid changes. The nodal active/reactive power injections during sub-slot t and scenario s, i.e. P_{its} and Q_{its}, consists of two terms:

$$P_{its} = \widehat{\mathrm{P}}_{it} + \Delta P_{its} \qquad \forall i \in \mathbb{B}, \forall t \in \mathbb{T}, \forall s \in \mathbb{S}, \quad (3)$$

$$Q_{its} = \widehat{\mathrm{Q}}_{it} + \Delta Q_{its} \qquad \forall i \in \mathbb{B}, \forall t \in \mathbb{T}, \forall s \in \mathbb{S}. \quad (4)$$

1) $\widehat{\mathrm{P}}_{it}$ and $\widehat{\mathrm{Q}}_{it}$ indicate the *expected* (i.e., combination of the *forecasted* and/or *planned* values) nodal active/reactive power injections during sub-slot t:

$$\widehat{\mathrm{P}}_{it} = -\widehat{\mathrm{P}}_{it}^{\mathrm{D}} + \sum_{k \in \mathbb{DDG}_i} \widehat{\mathrm{P}}_{k}^{\mathrm{DDG}} + \sum_{h \in \mathbb{RDG}_i} \widehat{\mathrm{P}}_{ht}^{\mathrm{RDG}} \qquad \forall i \in \mathbb{B}, \forall t \in \mathbb{T}, \quad (5)$$

$$\widehat{\mathrm{Q}}_{it} = -\widehat{\mathrm{Q}}_{it}^{\mathrm{D}} + \sum_{k \in \mathbb{DDG}_i} \widehat{\mathrm{Q}}_{k}^{\mathrm{DDG}} + \sum_{h \in \mathbb{RDG}_i} \widehat{\mathrm{Q}}_{h}^{\mathrm{RDG}} \qquad \forall i \in \mathbb{B}, \forall t \in \mathbb{T}, \quad (6)$$

2) ΔP_{its} and ΔQ_{its} respectively indicate the nodal active/reactive power deviations from $\widehat{\mathrm{P}}_{it}$ and $\widehat{\mathrm{Q}}_{it}$ during sub-slot t and scenario s:

$$\Delta P_{its} = -\Delta \mathrm{P}_{its}^{\mathrm{D}} + \sum_{k \in \mathbb{DDG}_i} f_{k}^{\mathrm{DDG,P}} + \sum_{h \in \mathbb{RDG}_i} \Delta \mathrm{P}_{hts}^{\mathrm{RDG}} + a_{ESS}\, f_{ts}^{\mathrm{ESS,P}} \qquad \forall i \in \mathbb{B}, \forall t \in \mathbb{T}, \forall s \in \mathbb{S}, \quad (7)$$

$$\Delta Q_{its} = -\Delta \mathrm{Q}_{its}^{\mathrm{D}} + \sum_{k \in \mathbb{DDG}_i} f_{k}^{\mathrm{DDG,Q}} + \sum_{h \in \mathbb{RDG}_i} f_{h}^{\mathrm{RDG,Q}} \qquad \forall i \in \mathbb{B}, \forall t \in \mathbb{T}, \forall s \in \mathbb{S}, \quad (8)$$

where a_{ESS} is a constant parameter equal to 1 if $i = 1$ and 0 otherwise. The linearized power flow model [12] is leveraged to derive the state of the ADN as a linear function of the nodal injections:

1) The Active/Reactive Power Flow at the PCC

The active power flow at the PCC during sub-slot t and scenario s can be expressed as a linear function with constant coefficients $\mathbf{P}_{t}^{0}$, $\mathbf{P}_{it}^{\mathrm{P}}$ and $\mathbf{P}_{it}^{\mathrm{Q}}$ as:

$$P_{0'ts} = \mathbf{P}_{t}^{0} + \sum_{i \in \mathbb{B}} \left(\mathbf{P}_{it}^{\mathrm{P}}\, \Delta P_{its} + \mathbf{P}_{it}^{\mathrm{Q}}\, \Delta Q_{its} \right) \qquad \forall t \in \mathbb{T}, \forall s \in \mathbb{S}. \quad (9)$$

The reactive power flow at the PCC during sub-slot t and scenario s can be expressed as a linear function with constant coefficients $\mathbf{Q}_t^0$, $\mathbf{Q}_{it}^{\mathrm{P}}$ and $\mathbf{Q}_{it}^{\mathrm{Q}}$ as:

$$Q_{0'ts} = \mathbf{Q}_t^0 + \sum_{i \in \mathbb{B}} \left(\mathbf{Q}_{it}^{\mathrm{P}}\, \Delta P_{its} + \mathbf{Q}_{it}^{\mathrm{Q}}\, \Delta Q_{its}\right) \qquad \forall t \in \mathbb{T}, \forall s \in \mathbb{S}. \quad (10)$$

2) *Voltage Magnitude of the ADN nodes*

The voltage magnitude of node i during sub-slot t and scenario s can be expressed as a linear function with constant coefficients $\mathbf{V}_{it}^0$, $\mathbf{V}_{ijt}^{\mathrm{P}}$ and $\mathbf{V}_{ijt}^{\mathrm{Q}}$ as:

$$V_{its} = \mathbf{V}_{it}^0 + \sum_{j \in \mathbb{B}} \left(\mathbf{V}_{ijt}^{\mathrm{P}}\, \Delta P_{jts} + \mathbf{V}_{ijt}^{\mathrm{Q}}\, \Delta Q_{jts}\right) \qquad \forall i \in \mathbb{B}, \forall t \in \mathbb{T}, \forall s \in \mathbb{S}. \quad (11)$$

3) *Current Phasor of the ADN branches*

The real (respectively imaginary) part of the current phasor of branch l during sub-slot t and scenario s can be expressed as linear functions with constant coefficients $\mathbf{I}_{lt}^{0,\mathrm{Real}}$, $\mathbf{I}_{lit}^{\mathrm{P,Real}}$ and $\mathbf{I}_{lit}^{\mathrm{Q,Real}}$ (respectively $\mathbf{I}_{lt}^{0,\mathrm{Imag}}$, $\mathbf{I}_{lit}^{\mathrm{P,Imag}}$ and $\mathbf{I}_{lit}^{\mathrm{Q,Imag}}$) as:

$$I_{lts}^{\mathrm{Real}} = \mathbf{I}_{lt}^{0,\mathrm{Real}} + \sum_{i \in \mathbb{B}} \left(\mathbf{I}_{lit}^{\mathrm{P,Real}}\, \Delta P_{its} + \mathbf{I}_{lit}^{\mathrm{Q,Real}}\, \Delta Q_{its}\right) \qquad \forall l \in \mathbb{L}, \forall t \in \mathbb{T}, \forall s \in \mathbb{S}, \quad (12)$$

$$I_{lts}^{\mathrm{Imag}} = \mathbf{I}_{lt}^{0,\mathrm{Imag}} + \sum_{i \in \mathbb{B}} \left(\mathbf{I}_{lit}^{\mathrm{P,Imag}}\, \Delta P_{its} + \mathbf{I}_{lit}^{\mathrm{Q,Imag}}\, \Delta Q_{its}\right) \qquad \forall l \in \mathbb{L}, \forall t \in \mathbb{T}, \forall s \in \mathbb{S}, \quad (13)$$

It is noteworthy that the expressions (9)-(13) can accommodate both meshed and radial grids and their coefficients are functions of the grid admittance matrix, the voltage magnitude at the PCC (slack node), $\widehat{\mathrm{P}}_{it}$ and $\widehat{\mathrm{Q}}_{it}$ [12].

B) Modeling the Objective Function

The objective function is designed to satisfy as much as possible the targeted power flow at the PCC with minimum cost. It can be mathematically formulated as:

$$\min_{\xi} C_{0'}^{\mathrm{Imb}} + C^{\mathrm{ESS}} + \sum_{k \in \mathbb{DDG}} \left[C_k^{\mathrm{DDG,P+}} + C_k^{\mathrm{DDG,P-}}\right], \quad (14)$$

where ξ indicates the set of optimization variables as:

$$\xi = \{f_k^{\mathrm{DDG,P}}, f_k^{\mathrm{DDG,Q}}, f_h^{\mathrm{RDG,Q}}, f_{ts}^{\mathrm{ESS,P}}, P^{\mathrm{ESS,Restore}}, F_{ts}^{\mathrm{ESS,P}}, P_{0'ts}, Q_{0'ts}, V_{its}, I_{lts}^{\mathrm{Real}}, I_{lts}^{\mathrm{Imag}}\}. \quad (15)$$

The objective function (14) includes three parts:

1) *Penalizing the Imbalance of the ADN at the PCC*

The active and reactive power imbalances of the ADN at the PCC during sub-slot t and scenario s are:

$$P_{0'ts}^{\mathrm{Imb}} = P_{0'ts} - \mathrm{P}_{0'}^{\mathrm{Target}}, \qquad \forall t \in \mathbb{T}, \forall s \in \mathbb{S}, \quad (16)$$

$$Q_{0'ts}^{\mathrm{Imb}} = Q_{0'ts} - \mathrm{Q}_{0'}^{\mathrm{Target}}. \qquad \forall t \in \mathbb{T}, \forall s \in \mathbb{S}. \quad (17)$$

The proposed method tries to follow the targeted power flow at the PCC with minimum deviations throughout the time slot. Thus, it assigns a virtual cost to the active/reactive power imbalances as:

$$C_{0'}^{\mathrm{Imb}} = \pi_{0'}^{\mathrm{Imb,P}} \sum_{s \in \mathbb{S}} \sum_{t \in \mathbb{T}} \left|P_{0'ts}^{\mathrm{Imb}}\right| + \pi_{0'}^{\mathrm{Imb,Q}} \sum_{s \in \mathbb{S}} \sum_{t \in \mathbb{T}} \left|Q_{0'ts}^{\mathrm{Imb}}\right|, \quad (18)$$

where $\pi_{0'}^{\mathrm{Imb,P}}$ and $\pi_{0'}^{\mathrm{Imb,Q}}$ are virtual large weighting coefficients; operator $|.|$ denotes the absolute values of its argument.

2) Penalizing the deployed flexibility from the ESS

During the real-time operation, i.e. the second stage of the method, the ESS's flexibility is exploited to mitigate the imbalance at the PCC stemming from the forecast errors of loads and RDGs. To this end, the first stage accounts for the fact that the ESS should restore an adequate state of energy (SOE), whereby, it is empowered to provide flexibility during the real-time operation. The net required active power flexibility from the ESS to mitigate the imbalance at the PCC during sub-slot t and scenarios s, i.e. $f_{ts}^{\mathrm{ESS,P}}$, consists of two terms:

$$f_{ts}^{\mathrm{ESS,P}} = P^{\mathrm{ESS,Restore}} + F_{ts}^{\mathrm{ESS,P}} \qquad \forall t \in \mathbb{T}, \forall s \in \mathbb{S}, \quad (19)$$

where $P^{\mathrm{ESS,Restore}}$ is the positive or negative active power that the ESS is scheduled to exchange over the whole time slot to restore an adequate SOE. $F_{ts}^{\mathrm{ESS,P}}$ is the active power flexibility that the ESS is expected to inject during sub-slot t and scenario s, in addition to its scheduled set-point $P^{\mathrm{ESS,Restore}}$, to mitigate the imbalance at the PCC. Actually, the method aims at maintaining the SOE close to the middle between its maximum, i.e. $\mathrm{SOE}^{\mathrm{ESS,Max}}$, and minimum, i.e. $\mathrm{SOE}^{\mathrm{ESS,Min}}$, allowed values by defining the targeted active power schedule of the ESS, i.e. $\mathrm{P}^{\mathrm{ESS,Target}}$, as:

$$\Delta\mathrm{SOE}^{\mathrm{ESS,Target}} = \mathrm{SOE}_0^{\mathrm{ESS}} - \frac{\mathrm{SOE}^{\mathrm{ESS,Max}} + \mathrm{SOE}^{\mathrm{ESS,Min}}}{2} \quad (20)$$

$$\mathrm{P}^{\mathrm{ESS,Target}} = \begin{cases} \dfrac{60}{\mathrm{T}\eta^{+}} \Delta\mathrm{SOE}^{\mathrm{ESS,Target}} & \Delta\mathrm{SOE}^{\mathrm{ESS,Target}} \le 0, \\ \dfrac{60\eta^{-}}{\mathrm{T}} \Delta\mathrm{SOE}^{\mathrm{ESS,Target}} & \Delta\mathrm{SOE}^{\mathrm{ESS,Target}} \ge 0. \end{cases} \quad (21)$$

where $\Delta\mathrm{SOE}^{\mathrm{ESS,Target}}$ is the difference between the initial SOE, i.e. $\mathrm{SOE}_0^{\mathrm{ESS}}$, and the average of $\mathrm{SOE}^{\mathrm{ESS,Min}}$ and $\mathrm{SOE}^{\mathrm{ESS,Max}}$. η^{+} and η^{-} are the charging and discharging efficiency of the ESS, respectively. Multiplier $\frac{1}{T/60}$ converts the duration of the time slot from minute to hour. In sum, the first stage tries to minimize the required active power flexibility from the ESS during the second stage, i.e. $F_{ts}^{\mathrm{ESS,P}}$, and to keep $P^{\mathrm{ESS,Restore}}$ close to its targeted value, i.e. $\mathrm{P}^{\mathrm{ESS,Target}}$. These two goals are achieved by defining the virtual cost:

$$C^{\mathrm{ESS}} = \pi^{\mathrm{ESS,P}} \sum_{s\in\mathbb{S}} \sum_{t\in\mathbb{T}} \left|F_{ts}^{\mathrm{ESS,P}}\right| + \pi^{\mathrm{ESS,SOE}} \left|P^{\mathrm{ESS,Restore}} - \mathrm{P}^{\mathrm{ESS,Target}}\right| + \sum_{s\in\mathbb{S}} \sum_{t\in\mathbb{T}} \gamma_{ts}^{\mathrm{ESS,Pnet}}, \quad (22)$$

where $\pi^{\mathrm{ESS,P}}$ and $\pi^{\mathrm{ESS,SOE}}$ are virtual weighting coefficients. The third term, i.e. $\gamma_{ts}^{\mathrm{ESS,Pnet}}$, is an auxiliary variable defined to support the linear model of the evolution of the SOE over time, as detailed in (34) and (47).

In order to prevent the expected power flexibilities $F_{ts}^{\mathrm{ESS,P}}$ to compete with the power flexibilities from the DDGs as a contribution to the power flexibility request of the TSO, the weighting coefficient $\pi^{\mathrm{ESS,P}}$ must be large in comparison to the DDG flexibility offer prices. In addition, the average of $F_{ts}^{\mathrm{ESS,P}}$ over all scenarios is enforced to be zero, thereby:

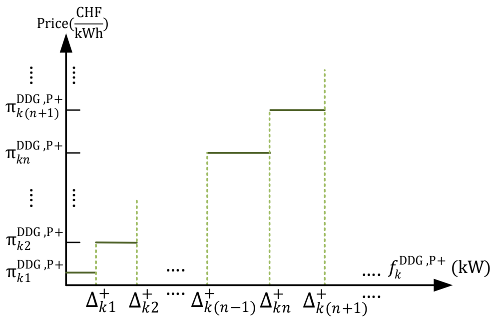

CHF, i.e. Confederation Helvetica Franc, is the currency of Switzerland.

Fig. 3 Offer curve of DDG k for upward active power flexibility provision.

$$\frac{1}{\mathrm{N}_s}\sum_{s\in\mathbb{S}} F_{ts}^{\mathrm{ESS,P}} = 0 \qquad \forall t\in\mathbb{T}, \qquad (23)$$

where N_s is the number of scenarios belonging to $\mathbb{S}$. This constraint helps to avoid a constant offset of $F_{ts}^{\mathrm{ESS,P}}$ all along the whole time slot. In the same time, it allows as well to preserve for some extent the SOE of the ESS. It is notable that (19), (22) and (23) enforce the average of the ESS's net provided active power flexibility, i.e. $f_{ts}^{\mathrm{ESS,P}}$, over all scenario to be a constant value equal to $\mathrm{P}^{\mathrm{ESS,Target}}$. Thus, its SOE is expected to remain close to the middle.

3) Cost of ADN Operator for Flexibility Procurement from DERs

The provided active power flexibility of DDG k, i.e. $f_k^{\mathrm{DDG,P}}$, can be divided into two non-negative components called upward, i.e. $f_k^{\mathrm{DDG,P+}}$, and downward, i.e. $f_k^{\mathrm{DDG,P-}}$, as:

$$f_k^{\mathrm{DDG,P}} = f_k^{\mathrm{DDG,P+}} - f_k^{\mathrm{DDG,P-}} \qquad \forall k\in\mathbb{DDG}, \qquad (24)$$

Each DDG offers its prices for the upward and downward active power flexibility provision to the ADN operator through two separate offer curves. For instance, the offer curve of DDG k for its upward active power flexibility is shown in Fig. 3 where n is the index for the offered blocks of DDG k; $\pi_{kn}^{\mathrm{DDG,P+}}$ is the price over the nth block; $\Delta_{k(n-1)}^{+}$ and Δ_{kn}^{+} are the beginning and the end of the nth block.

The area under the offer curve defines $C_k^{\mathrm{DDG,P+}}$ indicating the cost that the ADN operator pays to DDG k to procure $f_k^{\mathrm{DDG,P+}}$ for one hour. $C_k^{\mathrm{DDG,P+}}$ is a piecewise linear function of $f_k^{\mathrm{DDG,P+}}$:

$$C_k^{\mathrm{DDG,P+}} = -\pi_{kn}^{\mathrm{DDG,P+}}\Delta_{k(n-1)}^{+} + \sum_{n'=1}^{n-1}\pi_{kn'}^{\mathrm{DDG,P+}}\Delta_{kn'}^{+} + \pi_{kn}^{\mathrm{DDG,P+}} f_k^{\mathrm{DDG,P+}}$$
$$\Delta_{k(n-1)}^{+}\le f_k^{\mathrm{DDG,P+}} \le \Delta_{kn}^{+}, \quad \forall n, \quad (25)$$

where n' is the index for the offered blocks of DDG k. In the same way, $C_k^{\mathrm{DDG,P-}}$ can be calculated as:

$$C_k^{\mathrm{DDG,P-}} = -\pi_{kn}^{\mathrm{DDG,P-}}\Delta_{k(n-1)}^{-} + \sum_{n'=1}^{n-1}\pi_{kn'}^{\mathrm{DDG,P-}}\Delta_{kn'}^{-} + \pi_{kn}^{\mathrm{DDG,P-}} f_k^{\mathrm{DDG,P-}}$$
$$\Delta_{k(n-1)}^{-}\le f_k^{\mathrm{DDG,P-}} \le \Delta_{kn}^{-}, \quad \forall n. \quad (26)$$

The second part of the objective function (14) aims at minimizing $C_k^{\mathrm{DDG,P+}}$ and $C_k^{\mathrm{DDG,P-}}$ which are positive increasing functions. Thus, the optimum solution entails that only one of the two variables $f_k^{\mathrm{DDG,P+}}$ and $f_k^{\mathrm{DDG,P-}}$ can be nonzero. In other words, $f_k^{\mathrm{DDG,P+}}$ and $f_k^{\mathrm{DDG,P-}}$ are complementary variables and DDG k can provide either upward or downward active power flexibility (not both simultaneously).

In regard to the reactive power flexibility, it is assumed that the ADN operator has long-term contracts with DERs and can procure their reactive power flexibility without any additional cost. Thus, the reactive power flexibility procurements from DDGs and RDGs causes no cost.

C) Equivalent Linear Objective Function

The objective function (14) includes nonlinear parts defined in (18) and (22) along with a piecewise linear part defined in (25) and (26). This combination leads to a nonlinear piecewise objective function. However, all parts have equivalent linear optimization problems [13]. In the following, the equivalent linear optimization problem of each part is introduced:

1) Equivalent Linear Optimization Problem of (18)

Minimizing the first part of (14), i.e. (18), is equivalent to:

$$\min \pi_{0'}^{\mathrm{Imb,P}} \sum_{s\in\mathbb{S}} \sum_{t\in\mathbb{T}} \gamma_{0'ts}^{\mathrm{Imb,P}} + \pi_{0'}^{\mathrm{Imb,Q}} \sum_{s\in\mathbb{S}} \sum_{t\in\mathbb{T}} \gamma_{0'ts}^{\mathrm{Imb,Q}}, \tag{27}$$

subject to

$$-\gamma_{0'ts}^{\mathrm{Imb,P}} \le P_{0'ts}^{\mathrm{Imb}} \le \gamma_{0'ts}^{\mathrm{Imb,P}} \qquad \forall t \in \mathbb{T}, \forall s \in \mathbb{S}, \tag{28}$$

$$-\gamma_{0'ts}^{\mathrm{Imb,Q}} \le Q_{0'ts}^{\mathrm{Imb}} \le \gamma_{0'ts}^{\mathrm{Imb,Q}} \qquad \forall t \in \mathbb{T}, \forall s \in \mathbb{S}, \tag{29}$$

where $\gamma_{0'ts}^{\mathrm{Imb,P}}$ and $\gamma_{0'ts}^{\mathrm{Imb,Q}}$ are non-negative auxiliary variables.

2) Equivalent Linear Optimization Problem of (22)

Minimizing the second part of (14), i.e. (22), is equivalent to:

$$\min \pi^{\mathrm{ESS,P}} \sum_{s\in\mathbb{S}} \sum_{t\in\mathbb{T}} \gamma_{ts}^{\mathrm{ESS,P}} + \pi^{\mathrm{ESS,SOE}} \gamma^{\mathrm{ESS,SOE}} + \sum_{s\in\mathbb{S}} \sum_{t\in\mathbb{T}} \gamma_{ts}^{\mathrm{ESS,Pnet}}, \tag{30}$$

subject to

$$-\gamma_{ts}^{\mathrm{ESS,P}} \le F_{ts}^{\mathrm{ESS,P}} \le \gamma_{ts}^{\mathrm{ESS,P}} \qquad \forall t \in \mathbb{T}, \forall s \in \mathbb{S}, \tag{31}$$

$$P^{\mathrm{ESS,Restore}} - \mathrm{P}^{\mathrm{ESS,Target}} \le \gamma^{\mathrm{ESS,SOE}} \qquad \forall t \in \mathbb{T}, \forall s \in \mathbb{S}, \tag{32}$$

$$-\gamma^{\mathrm{ESS,SOE}} \le P^{\mathrm{ESS,Restore}} - \mathrm{P}^{\mathrm{ESS,Target}} \qquad \forall t \in \mathbb{T}, \forall s \in \mathbb{S}, \tag{33}$$

$$-\gamma_{ts}^{\mathrm{ESS,Pnet}} \le f_{ts}^{\mathrm{ESS,P}} \le \gamma_{ts}^{\mathrm{ESS,Pnet}} \qquad \forall t \in \mathbb{T}, \forall s \in \mathbb{S}, \tag{34}$$

where $\gamma_{ts}^{\mathrm{ESS,P}}$, $\gamma^{\mathrm{ESS,SOE}}$ and $\gamma_{ts}^{\mathrm{ESS,Pnet}}$ are non-negative auxiliary variables.

3) Equivalent Linear Optimization Problem of (25) and (26)

Minimizing the third part of (14), i.e. the sum of (25) and (26), is equivalent to:

$$\min \sum_{k\in\mathbb{DDG}} [\gamma_k^{\mathrm{DDG,P+}} + \gamma_k^{\mathrm{DDG,P-}}], \tag{35}$$

$$\frac{\mathrm{T}}{60} C_k^{\mathrm{DDG,P+}} \le \gamma_k^{\mathrm{DDG,P+}} \qquad \forall k \in \mathbb{DDG}, \tag{36}$$

$$\frac{\mathrm{T}}{60} C_k^{\mathrm{DDG,P-}} \le \gamma_k^{\mathrm{DDG,P-}} \qquad \forall k \in \mathbb{DDG}, \tag{37}$$

where multiplier $\frac{\mathrm{T}}{60}$ converts the cost during an hour, i.e. $C_k^{\mathrm{DDG,P+}}$ and $C_k^{\mathrm{DDG,P-}}$, to the cost during T minutes of a time slot; $\gamma_k^{\mathrm{DDG,P+}}$ and$\gamma_k^{\mathrm{DDG,P-}}$ are auxiliary variables.

The compact formulation of the equivalent linear objective function of (14) is presented below.

D) Linear Scenario-Based Optimization Problem Formulation

Based on the presented framework for modeling the state of the ADN and the cost incurred by the ADN operator, the optimal scheduling of DERs can be mathematically formulated as:

$$\min_{\xi'} \pi_{0'}^{\mathrm{Imb,P}} \sum_{s\in\mathbb{S}}\sum_{t\in\mathbb{T}} \gamma_{0'ts}^{\mathrm{Imb,P}} + \pi_{0'}^{\mathrm{Imb,Q}} \sum_{s\in\mathbb{S}}\sum_{t\in\mathbb{T}} \gamma_{0'ts}^{\mathrm{Imb,Q}} + \pi^{\mathrm{ESS,P}} \sum_{s\in\mathbb{S}}\sum_{t\in\mathbb{T}} \gamma_{ts}^{\mathrm{ESS,P}} + \pi^{\mathrm{ESS,SOE}} \gamma^{\mathrm{ESS,SOE}} + \sum_{s\in\mathbb{S}}\sum_{t\in\mathbb{T}} \gamma_{ts}^{\mathrm{ESS,Pnet}} + \sum_{k\in\mathbb{DDG}} \left[\gamma_k^{\mathrm{DDG,P+}} + \gamma_k^{\mathrm{DDG,P-}}\right], \tag{38}$$

subject to (7)-(13), (16), (17), (19), (23), (24)-(26), (28), (29), (31)-(34), (36) and (37) along with the constraints of the ADN and DERs introduced in (40), (42)-(47). ξ' indicates the set of optimization variables consisting of ξ, introduced in (15), and the auxiliary variables as:

$$\xi' = \xi \cup \{P_{0'ts}^{\mathrm{Imb}}, Q_{0'ts}^{\mathrm{Imb}}, f_k^{\mathrm{DDG,P+}}, f_k^{\mathrm{DDG,P-}}, \gamma_{0'ts}^{\mathrm{Imb,P}}, \gamma_{0'ts}^{\mathrm{Imb,Q}}, \gamma_{ts}^{\mathrm{ESS,P}}, \gamma^{\mathrm{ESS,SOE}}, \gamma_{ts}^{\mathrm{ESS,Pnet}}, \gamma_k^{\mathrm{DDG,P+}}, \gamma_k^{\mathrm{DDG,P-}}\}, \tag{39}$$

where operator ∪ calculates the union of two sets.

1) Modeling the Constraints of the ADN

Based on (11), the nodal voltage magnitude limits can be linearly expressed as:

$$\mathrm{V}_i^{\mathrm{Min}} \le V_{its} \le \mathrm{V}_i^{\mathrm{Max}} \qquad \forall i \in \mathbb{B}, \forall t \in \mathbb{T}, \forall s \in \mathbb{S}, \tag{40}$$

where $\mathrm{V}_i^{\mathrm{Min}}$ and $\mathrm{V}_i^{\mathrm{Max}}$ are the minimum and maximum voltage magnitude limit of node i.

Considering (12) and (13), the ampacity constraint of branch l[1] can be expressed as:

$${I_{lts}^{\mathrm{Real}}}^2 + {I_{lts}^{\mathrm{Imag}}}^2 \le \mathrm{I}_l^{\mathrm{Max}} \qquad \forall l \in \mathbb{L}, \forall t \in \mathbb{T}, \forall s \in \mathbb{S}, \tag{41}$$

where $\mathrm{I}_l^{\mathrm{Max}}$ is the maximum current flow limit of branch l. As shown in Fig. 4, the nonlinear constraint (41) can be approximated as a set of linear constraints with constant

coefficients $\mathbf{A}_{fl}^{\mathrm{Real}}, \mathbf{A}_{fl}^{\mathrm{Imag}}$ and $\mathbf{A}_{fl}^{0}$:

$$\mathbf{A}_{fl}^{\mathrm{Real}} I_{lts}^{\mathrm{Real}} + \mathbf{A}_{fl}^{\mathrm{Imag}} I_{lts}^{\mathrm{Imag}} \le \mathbf{A}_{fl}^{0} \qquad \forall l \in \mathbb{L}, \forall f \in \mathbb{A}_l, \forall t \in \mathbb{T}, \forall s \in \mathbb{S}, \tag{42}$$

where $\mathbb{A}_l$ is the set of linear constraints modeling the nonlinear ampacity constraint of branch l and f is the index for those linear constraints belonging to $\mathbb{A}_l$.

2) Modeling the Capability Area of DERs

To take advantage at most of the total available power flexibility of DERs, the proposed method considers the real nonlinear capability area of each DER and approximates it by using a set of linear boundaries. This approach is exemplified for a solar-PV generator, i.e. RDG, in Fig. 5. In this way, the capability area of DDG k can be expressed as a set of linear constraints with constant coefficients $\mathbf{D}_{km}^{0}, \mathbf{D}_{km}^{\mathrm{P}}$ and $\mathbf{D}_{km}^{\mathrm{Q}}$ as:

$$\mathbf{D}_{km}^{0} + \mathbf{D}_{km}^{\mathrm{P}} f_k^{\mathrm{DDG,P}} + \mathbf{D}_{km}^{\mathrm{Q}} f_k^{\mathrm{DDG,Q}} \le 0 \qquad \forall k \in \mathbb{DDG}, \forall m \in \mathbb{A}_k, \tag{43}$$

and the capability limits of RDG h can be expressed as a set of linear constraints with constant coefficients $\mathbf{R}_{hmts}^{0}, \mathbf{R}_{hmts}^{\mathrm{P}}$ and $\mathbf{R}_{hmts}^{\mathrm{Q}}$ as:

$$\mathbf{R}_{hmts}^{0} + \mathbf{R}_{hmts}^{\mathrm{P}} \Delta\mathrm{P}_{hts}^{\mathrm{RDG}} + \mathbf{R}_{hmts}^{\mathrm{Q}} f_h^{\mathrm{RDG,Q}} \le 0 \qquad \forall h \in \mathbb{RDG}, \forall m \in \mathbb{A}_h, \forall t \in \mathbb{T}, \forall s \in \mathbb{S}, \tag{44}$$

where $\mathbb{A}_k$ and $\mathbb{A}_h$ are the sets of linear constraints modeling the nonlinear capability area of DDG k and RDG h, respectively. m is the index for the linear constraints belonging to $\mathbb{A}_k$ or $\mathbb{A}_h$.

[1] The maximum current flow limit of branch l is modeled for its both sending and receiving ends.

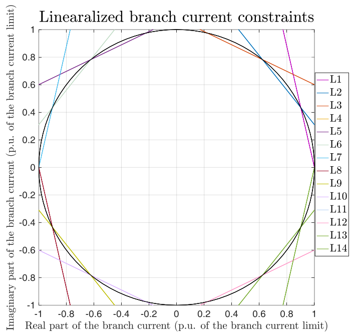

Fig. 4 Linearized ampacity constraint of a branch.

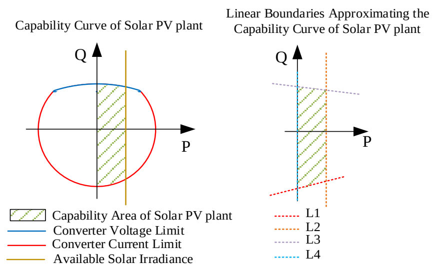

Fig. 5 Capability area of a solar-PV generator.

3) Modeling the Constraints of the Battery ESS

The power and energy limits of the ESS can be expressed as:

$$-\mathrm{P}^{\mathrm{ESS,Max}} \le f_{ts}^{\mathrm{ESS,P}} \le \mathrm{P}^{\mathrm{ESS,Max}} \qquad \forall t \in \mathbb{T}, \forall s \in \mathbb{S}, \quad (45)$$

$$\mathrm{SOE}^{\mathrm{ESS,Min}} \le SOE_{ts}^{\mathrm{ESS}} \le \mathrm{SOE}^{\mathrm{ESS,Max}} \qquad \forall t \in \mathbb{T}, \forall s \in \mathbb{S}, \quad (46)$$

where $\mathrm{P}^{\mathrm{ESS,Max}}$ is the ESS's rated power limit; SOE_{ts}^{ESS} is the ESS's SOE over sub-slot t and scenario s. The evolution of SOE_{ts}^{ESS} over time can be expressed as a linear function of $f_{ts}^{\mathrm{ESS,P}}$ and $\gamma_{ts}^{\mathrm{ESS,Pnet}}$ (the auxiliary variable defined in (30) and (34) characterizing the absolute value of $f_{ts}^{\mathrm{ESS,P}}$) [13]:

$$SOE_{ts}^{\mathrm{ESS}} = \mathrm{SOE}_0^{\mathrm{ESS}} + \frac{\tau_1}{3600}\sum_{t'=1}^{t} \eta^{+}\left[\frac{\gamma_{t's}^{\mathrm{ESS,Pnet}} - f_{t's}^{\mathrm{ESS,P}}}{2}\right] - \frac{\tau_1}{3600}\sum_{t'=1}^{t} \frac{1}{\eta^{-}}\left[\frac{\gamma_{t's}^{\mathrm{ESS,Pnet}} + f_{t's}^{\mathrm{ESS,P}}}{2}\right] \qquad \forall t \in \mathbb{T}, \forall s \in \mathbb{S}. \quad (47)$$

1.4.3. Second Stage: Real-Time Control

The second stage of the method starts at the beginning of the time slot and lasts until the end of the time slot, as shown in Fig. 1. This stage is designated to mitigate the impact of the mismatch between the forecasted consumption/generation of loads/RDGs and the realized ones on the active/reactive power imbalance at the PCC. Relying on a linear optimization problem, it controls the active/reactive power injections of the ESS to track the targeted active/reactive power flow at the PCC, i.e. $\mathrm{P}_{0'}^{\mathrm{Target}}$ and $\mathrm{Q}_{0'}^{\mathrm{Target}}$, while respecting the operational constraints of the ESS. The outlines of the control strategy are:

1- The whole time slot is split into N_{κ} time-intervals with duration τ_2 and κ is the index for time-intervals.
2- The scheduled set-point of ESS during each time-interval κ can be retrieved from the value of $P^{\mathrm{ESS,Restore}}$ determined at the first stage:
$$\widehat{\mathrm{P}}_{\kappa}^{\mathrm{ESS}} = P^{\mathrm{ESS,Restore}} \qquad \kappa = 1, \ldots, \mathrm{N}_{\kappa}, \quad (48)$$
3- The control strategy is executed at the beginning of each time-interval κ. The control action consists in determining and actuating the additional active and reactive powers flexibility, with respect to the scheduled set-point $\widehat{\mathrm{P}}_{\kappa}^{\mathrm{ESS}}$, that the ESS should provide during the current time-interval κ, i.e. $F_{\kappa}^{\mathrm{ESS,P}}$ and $F_{\kappa}^{\mathrm{ESS,Q}}$. They are constant values over the whole time-interval κ.
4- At the beginning of the time-interval κ, the most recent realized active/reactive powers flow at the PCC, i.e. $\mathrm{P}_{0'(\kappa-1)}$ and $\mathrm{Q}_{0'(\kappa-1)}$ are measured. Moreover, the actuated active/reactive powers flexibility of the ESS, i.e. $\widehat{\mathrm{P}}_{\kappa}^{\mathrm{ESS}} + \mathrm{F}_{(\kappa-1)}^{\mathrm{ESS,P}}$ and $\mathrm{F}_{(\kappa-1)}^{\mathrm{ESS,Q}}$, during the

previous time-interval $\kappa-1$ are known based on the the outcome of the accomplished control over time-interval $\kappa-1$. Therefore, the net realized active/reactive power absorption of the ADN excluding ESS, i.e. $\mathrm{P}_{(\kappa-1)}^{\mathrm{ADN}}$ and $\mathrm{Q}_{(\kappa-1)}^{\mathrm{ADN}}$ can be easily calculated as:

$$\mathrm{P}_{(\kappa-1)}^{\mathrm{ADN}}=\mathrm{P}_{0'(\kappa-1)}+\widehat{\mathrm{P}}_{(\kappa-1)}^{\mathrm{ESS}}+\mathrm{F}_{(\kappa-1)}^{\mathrm{ESS,P}} \tag{49}$$

$$\mathrm{Q}_{(\kappa-1)}^{\mathrm{ADN}}=\mathrm{Q}_{0'(\kappa-1)}+\mathrm{F}_{(\kappa-1)}^{\mathrm{ESS,Q}} \tag{50}$$

whereby the net realized active/reactive power absorption of the ADN during the time-interval κ is predicted to be equal to the one realized in the former time-interval. Thus, the active/reactive power flow at PCC during the time-interval κ is predicted to be:

$$P_{0'\kappa}=\mathrm{P}_{(\kappa-1)}^{\mathrm{ADN}}-\widehat{\mathrm{P}}_{\kappa}^{\mathrm{ESS}}-F_{\kappa}^{\mathrm{ESS,P}} \tag{51}$$

$$Q_{0'\kappa}=\mathrm{Q}_{(\kappa-1)}^{\mathrm{ADN}}-F_{\kappa}^{\mathrm{ESS,Q}} \tag{52}$$

To mathematically formulate the control strategy, let us assume to be at the beginning of the time-interval κ. The control objective is to keep $P_{0'\kappa}$ and $Q_{0'\kappa}$ close to $\mathrm{P}_{0'}^{\mathrm{Target}}$ and $\mathrm{Q}_{0'}^{\mathrm{Target}}$, respectively. This control objective can be formulated as:

$$\min_{\psi_\kappa}\ \pi_{0'}^{\mathrm{Imb,P}}\left|P_{0'\kappa}-\mathrm{P}_{0'}^{\mathrm{Target}}\right|+\pi_{0'}^{\mathrm{Imb,Q}}\left|Q_{0'\kappa}-\mathrm{Q}_{0'}^{\mathrm{Target}}\right|+\gamma_{\kappa}^{\mathrm{ESS,Pnet}}, \tag{53}$$

where $\pi_{0'}^{\mathrm{Imb,P}}$ and $\pi_{0'}^{\mathrm{Imb,Q}}$ are weighting coefficients; the third term, i.e. $\gamma_{\kappa}^{\mathrm{ESS,Pnet}}$, is a non-negative auxiliary variable defined to linearly model the evolution of the SOE over time-interval κ, as detailed in (55), (58) and (62); ψ_κ indicates the set of control variables as:

$$\psi_\kappa=\{F_{\kappa}^{\mathrm{ESS,P}},F_{\kappa}^{\mathrm{ESS,Q}}\}. \tag{54}$$

The nonlinear objective function (53) has an equivalent linear optimization problem as:

$$\min_{\psi_\kappa}\ \pi_{0'}^{Imb,P}\gamma_{\kappa}^{Imb,P}+\pi_{0'}^{Imb,Q}\gamma_{\kappa}^{Imb,Q}+\gamma_{\kappa}^{ESS,Pnet}, \tag{55}$$

subject to

$$-\gamma_{\kappa}^{\mathrm{Imb,P}}\le P_{0'\kappa}-\mathrm{P}_{0'}^{\mathrm{Target}}\le\gamma_{\kappa}^{\mathrm{Imb,P}} \tag{56}$$

$$-\gamma_{\kappa}^{\mathrm{Imb,Q}}\le Q_{0'\kappa}-\mathrm{Q}_{0'}^{\mathrm{Target}}\le\gamma_{\kappa}^{\mathrm{Imb,Q}} \tag{57}$$

$$-\gamma_{\kappa}^{\mathrm{ESS,Pnet}}\le\widehat{\mathrm{P}}_{\kappa}^{\mathrm{ESS}}+F_{\kappa}^{\mathrm{ESS,P}}\le\gamma_{\kappa}^{\mathrm{ESS,Pnet}} \tag{58}$$

where $\gamma_{\kappa}^{\mathrm{Imb,P}}$, $\gamma_{\kappa}^{\mathrm{Imb,Q}}$ are non-negative auxiliary variables.

The power limit of the ESS can be expressed as:

$$(\widehat{\mathrm{P}}_{\kappa}^{\mathrm{ESS}}+F_{\kappa}^{\mathrm{ESS,P}})^2+{F_{\kappa}^{\mathrm{ESS,Q}}}^2\le\mathrm{P}^{\mathrm{ESS,Max}} \tag{59}$$

similar to the approach adopted for linearizing constraint (41) and depicted in Fig. 4 the nonlinear constraint (59) can be expressed as a set of linear constraints with constant coefficients $\mathbf{E}_m^0$, $\mathbf{E}_m^{\mathrm{P}}$ and $\mathbf{E}_m^{\mathrm{Q}}$ as:

$$\mathbf{E}_m^0+\mathbf{E}_m^{\mathrm{P}}(\widehat{\mathrm{P}}_{\kappa}^{\mathrm{ESS}}+F_{\kappa}^{\mathrm{ESS,P}})+\mathbf{E}_m^{\mathrm{Q}}F_{\kappa}^{\mathrm{ESS,Q}}\le 0\quad\forall m\in\mathbb{A}_e, \tag{60}$$

where $\mathbb{A}_e$ is the set of linear constraints modeling the nonlinear maximum power constraint of the ESS, m is the index for the linear constraints belonging to $\mathbb{A}_e$.

The energy limits of the ESS can be modeled as:

$$\mathrm{SOE}^{\mathrm{ESS,Min}}\le SOE_{\kappa}^{\mathrm{ESS}}\le\mathrm{SOE}^{\mathrm{ESS,Max}} \tag{61}$$

The evolution of $SOE_{\kappa}^{\mathrm{ESS}}$ over time-interval κ can be expressed as a linear function of $\widehat{\mathrm{P}}_{\kappa}^{\mathrm{ESS}}$, $F_{\kappa}^{\mathrm{ESS,P}}$ and $\gamma_{\kappa}^{\mathrm{ESS,Pnet}}$ (the auxiliary variable defined in (53), (55) and (58) characterizing the

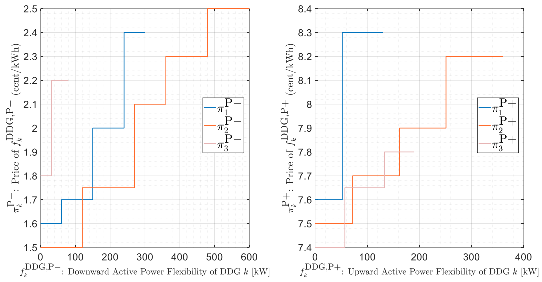

Fig. 6 Offer curve of DDGs for active power flexibility provision.

absolute value of $\widehat{\mathrm{P}}_{\kappa}^{\mathrm{ESS}} + F_{\kappa}^{\mathrm{ESS,P}}$) [13]:

$$SOE_{\kappa}^{\mathrm{ESS}} = \mathrm{SOE}_{\kappa-1}^{\mathrm{ESS}} + \frac{\tau}{3600}\eta^{+}\left[\frac{\gamma_{\kappa}^{\mathrm{ESS,Pnet}} - \widehat{\mathrm{P}}_{\kappa}^{\mathrm{ESS}} - F_{\kappa}^{\mathrm{ESS,P}}}{2}\right] - \frac{\tau}{3600}\frac{1}{\eta^{-}}\left[\frac{\gamma_{\kappa}^{\mathrm{ESS,Pnet}} + \widehat{\mathrm{P}}_{\kappa}^{\mathrm{ESS}} + F_{\kappa}^{\mathrm{ESS,P}}}{2}\right]. \quad (62)$$

The objective function (55) subject to (51), (52), (56)-(58), (60)-(62) forms a linear optimization problem whose the solution determines the set-point of the ESS over the time-interval κ.

1.5. Regulatory and legal barriers for implementation

- The DSO needs to have a battery energy storage to mitigate the impact of the mismatch between the forecasted consumption/generation of loads/RDGs and the realized ones on the active/reactive power imbalance at the PCC. It is notable that under the current regulation, DSOs cannot own battery energy storage.
- The DSO needs to develop a local flexibility market where all DERs can offer their active and reactive powers flexibility. However, this local flexibility market is allowed under the new revision of the Act on the Electricity supply but details need still to be clarified.

2. Achievement of deliverable:

2.1. Date

September 2020

2.2. Demonstration of the deliverable

The performance of the method is validated considering a real ADN located in the city of Aigle in southwest of Switzerland, as shown in Fig. 2. It includes 55 buses at 21 kV accommodating 2700 kWp installed solar PV units (RDGs), 910 kW installed hydropower units (DDGs) and a 720 kVA/500 kWh Lithium Titanate ESS with charging (discharging) efficiency of 94% (96%). The offer curves of DDGs are shown in Fig. 6, where indices 1, 2 and 3 refer to the DDGs connected to nodes 11, 53 and 55. Minimum and maximum of the nodal voltage magnitude limits are chosen

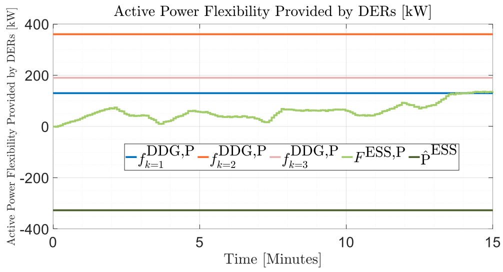

Fig. 7 Optimal required active power flexibility from DERs.

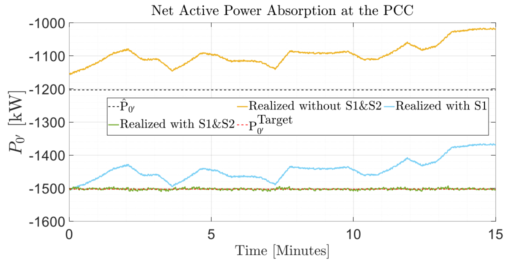

Fig.8 Realized active power flow at the PCC.

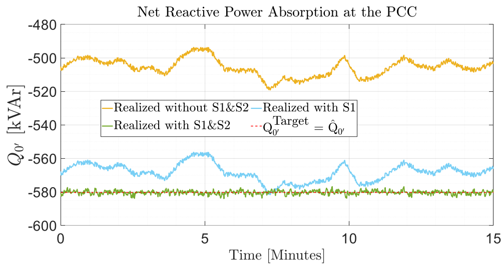

Fig. 9 Realized reactive power flow at the PCC.

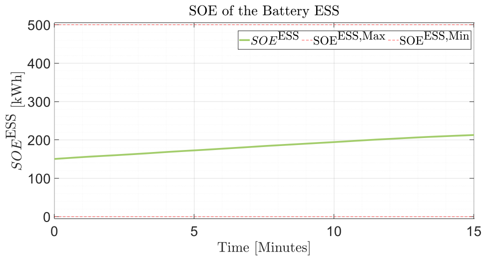

Fig. 10 Evolution of the ESS's SOE over the whole time slot.

as 0.95 p.u. and 1.05 p.u. In line with the timeline of the problem detailed in Fig. 1, t_{TSO}, t_{ADN}, T, τ_1 and τ_2 are considered 30 minutes, 15 minutes, 15 minutes, 30 seconds, 5 seconds respectively. The objective function's weighting coefficients $\pi_{0'}^{Imb,P}$, $\pi_{0'}^{Imb,Q}$, $\pi^{ESS,P}$ and $\pi^{ESS,SOE}$ are respectively assumed 100 cent/kW, 50 cent/kVAr, 30 cent/kW, 10 cent/kW, to prioritize different terms of the objective function for deploying the available local flexibility. Relying on the k-nearest neighbors algorithm [14], the scenarios required in the first stage of the method, i.e. $s \in \mathbb{S}$, are generated. Then, the problem is modeled by using YALMIP-MATLAB and solved with GUROBI solver.

For a case where SOE_0^{ESS}, $\hat{f}_{0'}^{P}$ and $\hat{f}_{0'}^{Q}$ are respectively set equal to 150 kWh (30%), -300 kW and 0 kVAr and the day-ahead forecast error[2] is assumed +10%, the required active power flexibility from DERs is shown in Fig. 7. Moreover, the realized active/reactive power flow at the PCC before/after applying the first stage (s1) and after applying both stages (s1 & s2) are shown in Fig. 8/ Fig.9. They illustrate the capability of the method for not only satisfying precisely the flexibility request of the TSO at the PCC but also mitigating the impact of the day-ahead forecast error on it. The evolution of the ESS's SOE over the whole time slot is shown in Fig. 10. As it can be seen, the method succeeded to move the ESS's SOE toward 250 kWh while mitigating the imbalance at the PCC.

The performance of the method over a whole day is investigated by applying it to the sunniest day of 2018, i.e 7th July, while the day-ahead forecast error[3] is assumed +10% and the

[2] Average over the whole time slot of the mismatch between ADN's realized active (reactive) power absorption and the day-ahead planned one.

[3] Average over the whole time slot of the mismatch between ADN's realized active (reactive) power absorption and the day-ahead planned one.

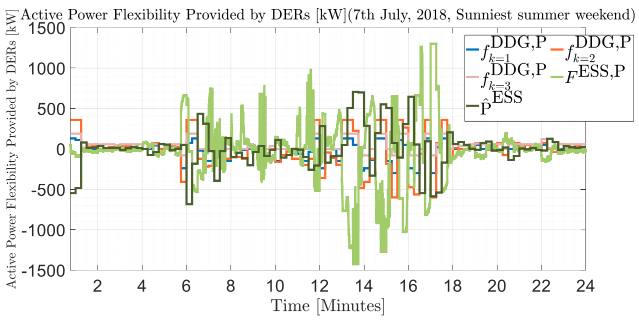

Fig. 11 Optimal required active power flexibility from DERs.

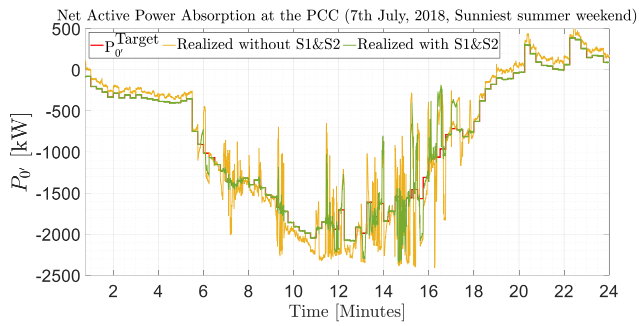

Fig. 12 Realized active power flow at the PCC.

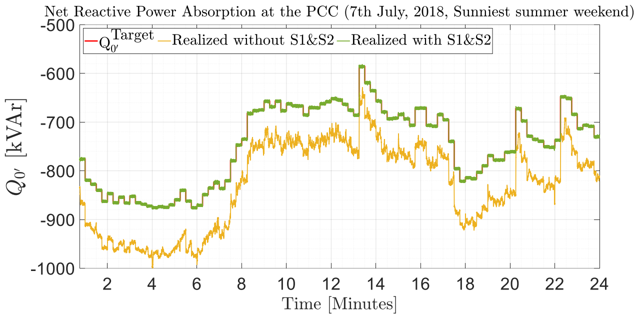

Fig. 13 Realized reactive power flow at the PCC.

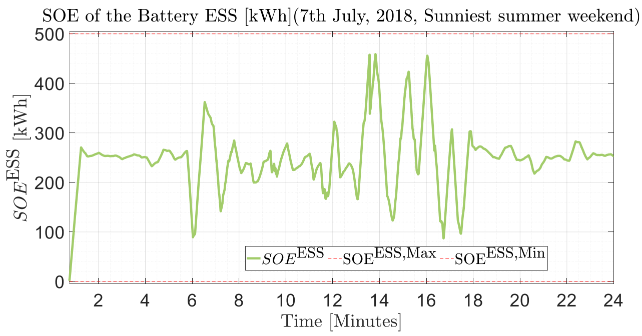

Fig. 14 Evolution of the ESS's state of energy (SOE) throughout the day.

active/reactyive power flexibility request of TSO is set at -100 kW and 0 kVAr. The required active power flexibility from DERs is shown in Fig. 11. The realized active/reactive power flow at the PCC before/after applying the first stage (s1) and after applying both stages (s1 & s2) are shown in Fig. 12 and Fig. 13. They illustrate the capability of the method for not only satisfying precisely the flexibility request of the TSO at the PCC but also mitigating the impact of the day-ahead forecast error on it. The evolution of the ESS's SOE over the whole time slot is shown in Fig. 14. As it can be seen, the method succeeded to move the ESS's SOE toward the middle, i.e. 250 kWh, while mitigating the imbalance at the PCC.

3. Impact

This deliverable introduced a method to optimally aggregate the power flexibility of DERs located in an ADN with the aim of providing active and reactive powers flexibility to the TSO. These active and reactive powers flexibility could deliver different services to the TSO such as congestion management, voltage control, secondary frequency control and tertiary frequency control. It is expected that a method of this kind facilitates the cooperation between TSO and DSO and improves the electric power system security of supply and reduces the cost associated to the ancillary services.

References

[1] International Renewable Energy Agency (IRENA), "Climate change and renewable energy", Jun. 2019, [Online]. Available: https://www.irena.org.
[2] Ottmar Edenhofer *et al.*, "Renewable energy sources and climate change mitigation", New York, Cambridge University Press, 2012.
[3] P. D. Redondo, and O. V. Vliet. "Modelling the energy future of Switzerland after the phase out of nuclear power plants." Energy Procedia, vol. 76, pp. 49-58, 2015.
[4] International Electrotechnical Commission (IEC), "Grid integration of large-capacity renewable energy source and use of large-capacity electrical energy storage," *White Paper,* Oct. 2012.
[5] M. CAILLIAU *et al*., EURELECTRIC, "Integrating Intermittent Renewable Sources in the EU Electricity System by 2020: Challenges and Solutions," 2010.
[6] L. Mehigan, J. P. Deane, B. P. O. Gallachóir, V. Bertsch, "A review of the role of distributed generation (DG) in future electricity systems," *Energy*, vol. 163, pp. 822-836, Nov. 2018.
[7] M. Heleno, R. Soares, J. Sumaili, R. Bessa, L. Seca, and M. Matos, "Estimation of the flexibility range in the transmission-distribution boundary," in *Proc. IEEE Power Tech*, Jun. 2015, pp. 1685-1691.
[8] J. P. Silva, J. Sumaili, R.J. Bessa, L. Seca, M. A. Matos, V. Miranda, M. Caujolle, B. Goncer, and M. Sebastian-Viana, "Estimating the active and reactive power flexibility area at the TSO-DSO interface," *IEEE Trans. Power Syst*., vol. 33, no. 5, pp. 4741–4750, Sep. 2018.
[9] F. Capitanescu, "TSO–DSO interaction: Active distribution network power chart for TSO ancillary services provision," *Elect. Power Syst. Res.*, vol. 163, pp. 226-230, Oct. 2018.
[10] M. Kalantar-Neyestanaki, F. Sossan, M. Bozorg, R. Cherkaoui, "Characterizing the Reserve Provision Capability Area of Active Distribution Networks: a Linear Robust Optimization Method", *IEEE Trans. Smart grid*, vol. 11, no. 3, pp. 2464-2475, May. 2020.
[11] G. Migliavacca, M. Rossi, D. Six, M. Džamarija, S. Horsmanheimo, C. Madina, I. Kockar, J. M. Morales, "SmartNet: H2020 project analyzing TSO–DSO interaction to enable ancillary services provision from distribution networks," *in Proc. 24th Int. Conf. CIRED*, Jun. 2017, pp. 1998-2002.
[12] A. Bernstein, and E. Dall Anese. "Linear power-flow models in multiphase distribution networks," in *Proc. IEEE Int. Conf. Innovative Smart Grid Technol.* (ISGT), Sep. 2017, pp.1-6.
[13] S. Boyd and L. Vandenberghe, *Convex Optimization*. Cambridge university press, 2004.
[14] Y. Chu and C. F. Coimbra, "Short-term probabilistic forecasts for direct normal irradiance," *Renewable Energy*, vol. 101, pp. 526-536, Feb. 2017.